Parametrising Temperature Dependent Properties in Thermal-Mechanical Analysis of Power Electronics Modules using Parametric Model Order Reduction

Sheikh Hassan[1)], Pushparajah Rajaguru[1)], Stoyan Stoyanov[1)] and Christopher Bailey[2)]
[1)]School of Computing and Mathematical Sciences, University of Greenwich, London, UK
[2)]School of Electrical, Computer and Energy Engineering, Arizona State University, Arizona, USA
s.r.hassan@greenwich.ac.uk

***Abstract*— In this paper, a direct-coupled thermal-mechanical analysis of a Power Electronics Modules (PEM) using ANSYS-FEM (Finite Element Method) is integrated with a Parametric Model Order Reduction (pMOR) technique. Unlike most present studies on model order reduction, which perform the coupled thermal-mechanical analysis by sequential-coupled thermal-mechanical models, the direct-coupled thermal-mechanical approach deployed in this study solves the thermal and structural models simultaneously. Commonly, pMOR mainly focuses on parametrising model parameters (e.g., material properties, loads.) that are constants. In this investigation, a new approach to parametrise temperature-dependent properties using pMOR, such as the coefficient of thermal expansion (CTE) of the materials in PEM structures, has been demonstrated in the context of the reliability assessment of electronic modules. A two-dimensional finite element model of a PEM is developed and used to study the temperature-dependent CTE effects of the Aluminium (Al) alloy on the thermal-mechanical response of the system under thermal load. A Krylov subspace-based technique, PRIMA, has been used for the model order reduction and a linear approach of matrix interpolation for the parametrisation in the pMOR. The full-order state-space model has 30,612 degrees of freedom (DOFs), and the reduced model achieved by pMOR has just 8 DOFs. The simulation runs show that with this approach, a substantial reduction in computational time can be achieved, for this problem, by 81% between the full and the reduced order models. In modelling predictions, the pMOR-based solution has retained the accuracy of results. In this instance, the average difference in stress result, compared to the ANSYS-FEM model (FOM) solution, is only 0.43%.**

Keywords—Finite Element Method (FEM), Thermal-Mechanical Analysis, Power Electronics Module (PEM), Reliability Assessment, Parametric Model Order Reduction (pMOR)

I. INTRODUCTION

With the advancement of modern technologies in disciplines such as space travel, aeronautics, and nuclear applications, it is becoming increasingly difficult for engineers to work on complex and expensive projects [1, 2]. These technologies require reliability assessments and protection constraints as these are essential for safety. Engineering analyses and designs are mainly done by simulating working principles of physical domains, and these simulations are based on mathematical models [3, 4]. Partial differential equations (PDEs), derived from engineering sciences, can explain the working principles of physical systems [5, 6]. The finite element method (FEM) is currently one of the most used computational tools for solving PDEs. PDEs are discretised into algebraic equations utilising simple approximate unknown variables in finite element analysis. The computation in finite element analysis includes complex and significantly high dimensional systems of differential equations. Reduction of dimensions of these equations is in high demand considering the application and simulation time requirements. The classic method of model reduction technique, Modal truncation, and most widely practised Krylov subspace-based techniques offer good approximate models [7, 8, 9]. However, as reported in previous studies, Krylov subspace-based techniques are comparatively "semi-automatic" [8].

Electronic systems' performances and reliability are reliant on thermal behaviours. One of the crucial means of dissipation in these systems is thermal-elastic damping. Hence, it is vital to concentrate on the thermal-mechanical analysis of electronic systems for reliability assessments.

Thermal-mechanical analysis-based reliability assessment had been previously conducted with FEM and CARES, a reliability assessment computational tool, by Eblen [10] for microelectronic package designing. Codecasa et al. [11] presented a computational tool, TRIC, a multigrid and ad-hoc projection-based solver to reduce simulation time for necessary thermal-mechanical analysis in electronic packaging. Shen and Ke [12] investigated an electrical contact region by electrical-thermal-mechanical coupled analysis.

Bai and Su [13] examined a large-scale model of a linear-drive multimode resonator by devising a Krylov subspace-based model reduction algorithm. Liu et al. [14] applied Krylov subspace-based model order reduction (MOR) technique to obtain the temperature profile of an electrical converter assembly used in hybrid and electric vehicles. Several works focused on developing boundary condition independent (BCI) reduced thermal and coupled models, and they used Krylov subspace-based approach [15] and a reduction matrix code, FANTASTIC [16, 17], to investigate multiple electronic systems.

A thermal-mechanical assessment of a micro-resonator had been performed by Choi et al. [18] before, where they applied the moment matching algorithm for Krylov subspace-based model reduction. Mechanical loading of an IGBT-PEM structure and electrical-thermal profiles of a PEM wire-bond structure were studied, through Krylov subspace-based MOR techniques, by Rajaguru et al. [9, 19].

A modal approach had been previously applied for model reduction of thermal models and optimisation of electronic boards by Bissuel et al. [20]. A frequency response analysis of a micro-thruster was performed by Baur et al. [21], utilising several pMOR methodologies to parametrise the physical properties of the model. Feng et al. [22] applied a multi-moment-matching based pMOR approach to electrical and electrical-thermal models of a nanoelectronics structure to parametrise a physical dimension of the model. Random variables of an electromagnetic-heat model were parametrised with a pMOR method, which follows the superposition principle, by ter Maten et al. [23]. A parametric reduced order model (ROM) of a piezoelectric energy harvester was developed by Bouhedma et al. [24] using Krylov subspace-based MOR technique to parametrise the geometric properties of the model. Three reduced-order modelling approaches were explored, by Schütz et al. [25], to parametrise magnetostatic variables of micro-actuator systems. Yuan et al. [26] applied two pMOR methods to build an optimised model of a miniaturised thermoelectric generator.

The FANTASTIC code was employed by Scognamillo et al. [27] for performing the electrical-thermal examination of a power module, where nonlinear thermal impacts were realised in the model. A procedure to achieve a reduced order model of a multi-physical piezoelectric kick and catch actuator system with nonlinear input had been presented by Schütz et al. [28] by using a Krylov subspace-based approach.

In most above-referenced studies, the coupled thermal-mechanical models had been solved by sequential-coupled models. But a direct-coupled thermal-mechanical model is more reasonable and provides more accurate results. Thus, a direct coupled thermal-mechanical model, which solves the thermal and mechanical models simultaneously, has been used for the current analysis. Furthermore, in previous pMOR studies, constant values of material properties, e.g., coefficient of thermal expansion (*CTE*), have been widely parametrised. But temperature-dependent properties of materials should be considered for more realistic thermal-mechanical parametric analysis. Hence, temperature-dependent *CTE* of the wire material for the current PEM structure has been parametrised in this pMOR study.

II. Problem Formulation

A. Parametric Full Order Model

The parametric state-space model can be expressed in the form [26, 29]:

$$\begin{aligned} \boldsymbol{E}(\boldsymbol{p}_i)\dot{\boldsymbol{x}}(\boldsymbol{p}_i,t) &= \boldsymbol{A}(\boldsymbol{p}_i)\boldsymbol{x}(\boldsymbol{p}_i,t) + \boldsymbol{B}(\boldsymbol{p}_i)\boldsymbol{u}(\boldsymbol{p}_i,t) \\ \boldsymbol{y}(\boldsymbol{p}_i,t) &= \boldsymbol{C}(\boldsymbol{p}_i)\boldsymbol{x}(\boldsymbol{p}_i,t) \end{aligned} \tag{1}$$

Here, $\boldsymbol{E}(\boldsymbol{p}_i), \boldsymbol{A}(\boldsymbol{p}_i) \in \mathbb{R}^{N\times N}$ are system matrices. $\boldsymbol{B}(\boldsymbol{p}_i) \in \mathbb{R}^{N\times M}$ and $\boldsymbol{C}(\boldsymbol{p}_i) \in \mathbb{R}^{P\times N}$ are input and output matrices; they are dependent on parametric points $\boldsymbol{p}_i$. $\boldsymbol{u}(\boldsymbol{p}_i,t) \in \mathbb{R}^M$ and $\boldsymbol{y}(\boldsymbol{p}_i,t) \in \mathbb{R}^P$ are inputs and outputs of the system, and $\boldsymbol{x}(\boldsymbol{p}_i,t) \in \mathbb{R}^N$ is the states of the system, they are time, t, and parametric point, $\boldsymbol{p}_i$, dependent. $\boldsymbol{p}_i$, here, is considered a vector of parametric points representing changes in modelling properties, for $i = 0, 1, \dots k$, with k parametric points.

B. Projection-based Model Order Reduction

The linear time-invariant (LTI) system, parametric point independent state-space model of (1), can be expressed in the form [26, 29]:

$$\begin{aligned} \boldsymbol{E}\,\dot{\boldsymbol{x}}(t) &= \boldsymbol{A}\,\boldsymbol{x}(t) + \boldsymbol{B}\,\boldsymbol{u}(t) \\ \boldsymbol{y}(t) &= \boldsymbol{C}\,\boldsymbol{x}(t) \end{aligned} \tag{2}$$

Here, $\boldsymbol{E}, \boldsymbol{A} \in \mathbb{R}^{N\times N}$ are system matrices. $\boldsymbol{B} \in \mathbb{R}^{N\times M}$ and $\boldsymbol{C} \in \mathbb{R}^{P\times N}$ are input and output matrices. $\boldsymbol{u}(t) \in \mathbb{R}^M$ and $\boldsymbol{y}(t) \in \mathbb{R}^P$ are the inputs and outputs of the system, and $\boldsymbol{x}(t) \in \mathbb{R}^N$ is the states of the system. $N \in \mathbb{N}$ represents the order of the system and is deemed to be very high.

The reduced order model of the system in (2) is then can be stated as [26, 29]:

$$\begin{aligned} \boldsymbol{E}_r\,\dot{\boldsymbol{x}}_r(t) &= \boldsymbol{A}_r\,\boldsymbol{x}_r(t) + \boldsymbol{B}_r\,\boldsymbol{u}_r(t) \\ \boldsymbol{y}_r(t) &= \boldsymbol{C}_r\,\boldsymbol{x}_r(t) \end{aligned} \tag{3}$$

The reduced matrices in (3) are determined as $\boldsymbol{E}_r = \boldsymbol{V}^T\boldsymbol{E}\boldsymbol{V}$, $\boldsymbol{A}_r = \boldsymbol{V}^T\boldsymbol{A}\boldsymbol{V}$, $\boldsymbol{B}_r = \boldsymbol{V}^T\boldsymbol{B}$ and $\boldsymbol{C}_r = \boldsymbol{C}\boldsymbol{V}$ using PRIMA [30, 31]. Here, $\boldsymbol{E}_r, \boldsymbol{A}_r \in \mathbb{R}^{q\times q}$, $\boldsymbol{B} \in \mathbb{R}^{q\times m}$ and $\boldsymbol{C} \in \mathbb{R}^{p\times q}$ matrices are dimensionally very small as the projection (transformation) matrix $\boldsymbol{V} \in \mathbb{R}^{N\times q}$ and $q \ll N$. The projection (transformation) matrix is achieved through the transfer function of the full order model (2), and then the transfer function of the reduced order model is calculated. Transfer functions of the full order model and reduced order model can be described as [30, 31]:

$$\boldsymbol{Y}(s) = \boldsymbol{C}\,(s\boldsymbol{E} - \boldsymbol{A}\,)^{-1}\boldsymbol{B} \tag{4}$$

$$\boldsymbol{Y}_r(s) = \boldsymbol{C}_r(s\boldsymbol{E}_r - \boldsymbol{A}_r)^{-1}\boldsymbol{B}_r \tag{5}$$

C. Interpolation of Sparse Matrices

Considering matrices in (1) as $\boldsymbol{X}(\boldsymbol{p}_i) = \boldsymbol{E}(\boldsymbol{p}_i)$, $\boldsymbol{A}(\boldsymbol{p}_i)$, $\boldsymbol{B}(\boldsymbol{p}_i)$ as sparse matrices, the state-space system for considered parametric points can be achieved by implementing linear matrix interpolation as shown below [29, 32, 33]:

$$\boldsymbol{X}(\boldsymbol{p}_i) = \boldsymbol{X}(\boldsymbol{p}_{i=0}) + \omega(\boldsymbol{p}_i)\,[\boldsymbol{X}(\boldsymbol{p}_{i=k}) - \boldsymbol{X}(\boldsymbol{p}_{i=0})] \tag{6}$$

Here, $\omega(\boldsymbol{p}_i)$ is calculated using the linear interpolation method. For current case, a bi-linear approach has been adopted to implement matrix interpolation. In the present study, $i = 0, 1, \dots, k$ with $k = 6$. So, the adopted bi-linear interpolation method can be expressed as:

$$\begin{aligned} \boldsymbol{X}\left(\boldsymbol{p}_{i=0,1,2,3}\right) &= \boldsymbol{X}(\boldsymbol{p}_0) + \omega(\boldsymbol{p}_i)\,\left[\boldsymbol{X}\left(\boldsymbol{p}_{\frac{k}{2}}\right) - \boldsymbol{X}(\boldsymbol{p}_0)\right] \\ \boldsymbol{X}\left(\boldsymbol{p}_{i=4,5,6}\right) &= \boldsymbol{X}\left(\boldsymbol{p}_{\frac{k}{2}}\right) + \omega(\boldsymbol{p}_i)\,\left[\boldsymbol{X}(\boldsymbol{p}_k) - \boldsymbol{X}\left(\boldsymbol{p}_{\frac{k}{2}}\right)\right] \end{aligned} \tag{7}$$

D. Parametric Reduced Order Model

Finally, the reduced parametric model can be formed using the interpolated matrices shown in (7) and following the approach shown in (3). The reduced parametric model can be expressed as [26]:

$$\begin{aligned} \boldsymbol{E}_r(\boldsymbol{p}_i)\dot{\boldsymbol{x}}_r(\boldsymbol{p}_i,t) &= \boldsymbol{A}_r(\boldsymbol{p}_i)\boldsymbol{x}_r(\boldsymbol{p}_i,t) \\ &\quad + \boldsymbol{B}_r(\boldsymbol{p}_i)\boldsymbol{u}_r(\boldsymbol{p}_i,t) \\ \boldsymbol{y}_r(\boldsymbol{p}_i,t) &= \boldsymbol{C}_r(\boldsymbol{p}_i)\boldsymbol{x}_r(\boldsymbol{p}_i,t) \end{aligned} \tag{8}$$

The reduced parametric model in (8) has been solved by using the generalised trapezoidal rule (GTR) [9].

E. Parametric Thermal-Mechanical Model

After finite element discretisation, the thermal-mechanical model studied in this work forms a second-order system. The

parametric thermal-mechanical model can be expressed as the followings [34, 35]:

$$\begin{aligned} \boldsymbol{M}(\boldsymbol{p}_i)\ddot{\boldsymbol{z}}(\boldsymbol{p}_i,t) + \boldsymbol{D}(\boldsymbol{p}_i)\dot{\boldsymbol{z}}(\boldsymbol{p}_i,t) + \boldsymbol{K}(\boldsymbol{p}_i)\boldsymbol{z}(\boldsymbol{p}_i,t) \\ = \boldsymbol{G}(\boldsymbol{p}_i)\boldsymbol{u}(\boldsymbol{p_i},t) \\ \boldsymbol{y}(\boldsymbol{p}_i,t) = \boldsymbol{L}(\boldsymbol{p}_i)\,\boldsymbol{z}(\boldsymbol{p}_i,t) \end{aligned} \tag{9}$$

Here, $\boldsymbol{M}(\boldsymbol{p}_i), \boldsymbol{D}(\boldsymbol{p}_i), \boldsymbol{K}(\boldsymbol{p}_i) \in \mathbb{R}^{n\times n}$ are mass, damping and stiffness matrices with $2n = N$. $\boldsymbol{G}(\boldsymbol{p}_i) \in \mathbb{R}^{n\times M}$ and $\boldsymbol{L}(\boldsymbol{p}_i) \in \mathbb{R}^{P\times n}$ are input and output matrices. $\boldsymbol{u}(\boldsymbol{p}_i,t) \in \mathbb{R}^{M}$ and $\boldsymbol{y}(\boldsymbol{p}_i,t) \in \mathbb{R}^{P}$ are the inputs and outputs of the system, and $\boldsymbol{z}(\boldsymbol{p}_i,t) \in \mathbb{R}^{n}$ is the states of the system. For a general direct-coupled thermal-mechanical analysis, matrices and vectors are defined as [35]:

$$\begin{aligned} &\boldsymbol{M} = \begin{bmatrix} \boldsymbol{M}_s & \boldsymbol{0} \\ \boldsymbol{0} & \boldsymbol{0} \end{bmatrix}, \boldsymbol{D} = \begin{bmatrix} \boldsymbol{D}_s & \boldsymbol{0} \\ \boldsymbol{D}^{tu} & \boldsymbol{D}^{t} \end{bmatrix}, \boldsymbol{K} = \begin{bmatrix} \boldsymbol{K}_s & \boldsymbol{K}^{ut} \\ \boldsymbol{0} & \boldsymbol{K}^{t} \end{bmatrix}, \\ &\boldsymbol{G} = \begin{bmatrix} \boldsymbol{F} \\ \boldsymbol{Q} \end{bmatrix}, \ddot{\boldsymbol{z}} = \begin{bmatrix} \ddot{\boldsymbol{z}}_{ut} \\ \ddot{\boldsymbol{T}} \end{bmatrix}, \dot{\boldsymbol{z}} = \begin{bmatrix} \dot{\boldsymbol{z}}_{ut} \\ \dot{\boldsymbol{T}} \end{bmatrix}, \boldsymbol{z} = \begin{bmatrix} \boldsymbol{z}_{ut} \\ \boldsymbol{T} \end{bmatrix} \end{aligned} \tag{10}$$

$$\text{with, } \boldsymbol{K}^t = \boldsymbol{K}^{tb} + \boldsymbol{K}^{tc}, \boldsymbol{F} = \boldsymbol{F}^{nd} + \boldsymbol{F}^{pr} + \boldsymbol{F}^{ac}, \boldsymbol{Q} = \boldsymbol{Q}^{nd} + \boldsymbol{Q}^{g} + \boldsymbol{Q}^{c} \tag{11}$$

Here, $\boldsymbol{M}_s$ is structural mass matrix. $\boldsymbol{D}_s$, $\boldsymbol{D}^t$ and $\boldsymbol{D}^{tu}$ are structural damping, thermal specific heat and thermoelastic damping matrices. $\boldsymbol{K}_s$, $\boldsymbol{K}^{ut}$ and $\boldsymbol{K}^t$ are structural stiffness, thermoelastic stiffness and thermal conductivity matrices with $\boldsymbol{K}^{tb}$ and $\boldsymbol{K}^{tc}$ as thermal conductivity matrices of material and convection surface. $\boldsymbol{F}$ is applied mechanical load vector with $\boldsymbol{F}^{nd}$, $\boldsymbol{F}^{pr}$ and $\boldsymbol{F}^{ac}$ as applied nodal force and applied pressure load vectors, and force vector because of acceleration effects. $\boldsymbol{z}_{ut}$ and $\boldsymbol{T}$ are displacement and thermal potential vector. $\boldsymbol{Q}$ is applied thermal load vector with $\boldsymbol{Q}^{nd}$, $\boldsymbol{Q}^{c}$ and $\boldsymbol{Q}^{g}$ as applied nodal heat flow rate and convection surface vectors, and heat generation rate vector excluding Joule heating.

The current thermal-mechanical model in (9) has been transformed to the state-space representation shown in (1) as [19, 34]:

$$\begin{aligned} &\begin{bmatrix} \boldsymbol{F} & \boldsymbol{0} \\ \boldsymbol{0} & \boldsymbol{M} \end{bmatrix} \begin{bmatrix} \dot{\boldsymbol{z}} \\ \ddot{\boldsymbol{z}} \end{bmatrix} = \begin{bmatrix} \boldsymbol{0} & \boldsymbol{F} \\ -\boldsymbol{K} & -\boldsymbol{D} \end{bmatrix} \begin{bmatrix} \boldsymbol{z} \\ \dot{\boldsymbol{z}} \end{bmatrix} + \begin{bmatrix} \boldsymbol{0} \\ \boldsymbol{G} \end{bmatrix} \boldsymbol{u} \\ &\boldsymbol{y} = [\boldsymbol{L} \quad \boldsymbol{0}] \begin{bmatrix} \boldsymbol{z} \\ \dot{\boldsymbol{z}} \end{bmatrix} \end{aligned} \tag{12}$$

$$\text{with, } \boldsymbol{E} = \begin{bmatrix} \boldsymbol{F} & \boldsymbol{0} \\ \boldsymbol{0} & \boldsymbol{M} \end{bmatrix}, \boldsymbol{A} = \begin{bmatrix} \boldsymbol{0} & \boldsymbol{F} \\ -\boldsymbol{K} & -\boldsymbol{D} \end{bmatrix}, \boldsymbol{B} = \begin{bmatrix} \boldsymbol{0} \\ \boldsymbol{G} \end{bmatrix}, \boldsymbol{C} = [\boldsymbol{L} \quad \boldsymbol{0}], \dot{\boldsymbol{x}} = \begin{bmatrix} \dot{\boldsymbol{z}} \\ \ddot{\boldsymbol{z}} \end{bmatrix}, \boldsymbol{x} = \begin{bmatrix} \boldsymbol{z} \\ \dot{\boldsymbol{z}} \end{bmatrix} \tag{13}$$

Here, $\boldsymbol{F} \in \mathbb{R}^{n\times n}$ must be a non-singular matrix. In the current modelling, $\boldsymbol{F} = \boldsymbol{I}_n$, where $\boldsymbol{I}_n$ is an $n \times n$ identity matrix.

III. Power Electronics Module

In this work, a *2D* model of a power electronics module (PEM) has been considered for a thermal-mechanical analysis. It is a *SiC*-based power module. Fig. 1 shows the PEM structure and boundary conditions used for the coupled analysis. The model was built in ANSYS with *Al* (alloy) as the wire material, and the material properties of *Al* (alloy) will be parametrised in this pMOR study.

A. FEM Model

A direct coupled transient thermal-mechanical analysis has been adopted for the FEM model. The *SiC* bodies of the model are thermal sources with isothermal boundary conditions of $T_{SiC} = 100^oC$. It is considered high temperature, labelled A in Fig. 1, in the model with the assigned uniform temperature value. The bottom edge of the baseplate, with *Cu* material, has an isothermal boundary condition of $T_B = 22^oC$. It is the low temperature of the model, labelled B in Fig. 1. This low temperature matches the initial and ambient temperatures of the model. For structural (mechanical) boundary conditions, the bottom two corner vertices are assumed to be rigidly fixed, i.e., no deformation is anticipated for these two vertices. The analysis time for the current model is $10s$, and the heat-generating body has a constant temperature throughout the analysis. Since no plasticity behaviour is considered for the wire material, *Al* (alloy), in the PEM structure, varying temperature behaviour of the heat-generating body has not been practised in the current analysis for the simplicity of the model.

B. Grid Independence Study

The FEM model has been reviewed for consistencies considering two different mesh sizes, according to the validation method in [36]. Fig. 2 shows the temperature and total deformation results, along a probing point (line/path), for two different mesh sizes. The probing point is a vertical line in the left part of the PEM structure, starting at the top of the wire, in the wire bond area, and proceeding to the bottom of the baseplate. The results for two different mesh sizes match very well. Mesh 1 has 5398 nodes with 4493 elements, and Mesh 2 has 3813 nodes with 3074 elements. Mesh 1 and Mesh 2 have an average orthogonal quality of 0.99, considered "outstanding" quality according to [36].

C. Parametric Points

The coefficient of thermal expansion of *Al* (alloy), CTE_{Al}, depends on temperature distribution in the *Al* (alloy) bodies, representing a non-linear material property for the material. This CTE_{Al} and Young's Modulus of *Al* (alloy), E_{Al}, have been parametrised in this work for design points exploration. Uniform parametric points, seen in Fig. 3, have been chosen

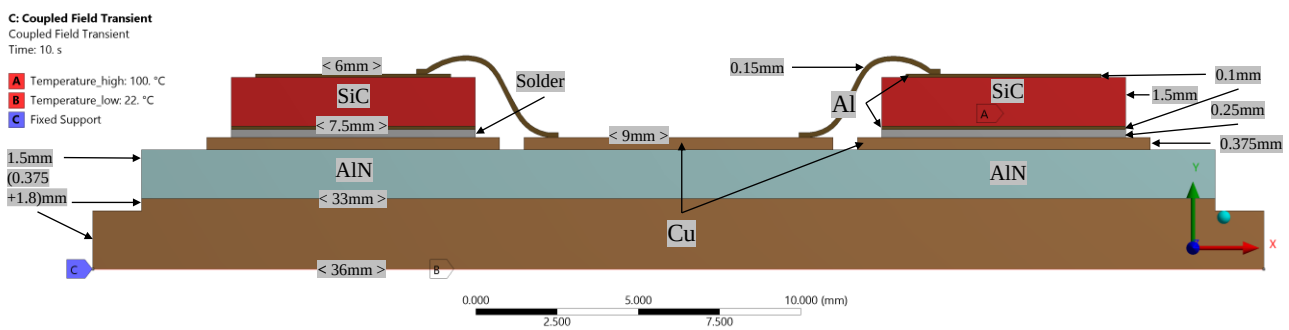

Figure 1: *2-D* PEM structure and Boundary Conditions.

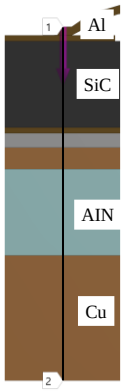

(a) Probing Point (Line/Path).

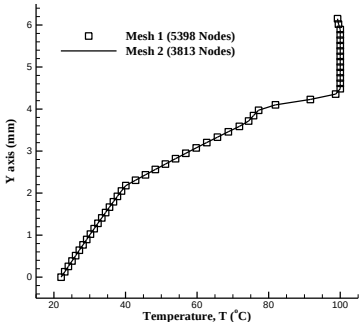

(b) Temperature, T

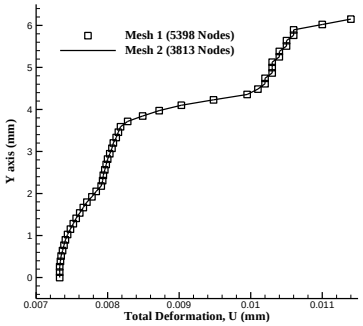

(c) Total Deformation, U

Figure 2: Mesh sensitivity analysis comparing temperature and total deformation along a probing point (line/path) in the left side of the PEM structure shown in Fig. 1.

to implement pMOR with matrix interpolation. The parametric points are equally spaced parametric points, i.e., CTE_{Al} values are uniformly spaced corresponding to their temperature, and E_{Al} constant values are also equally spaced. Fig. 4 shows the CTE_{Al} values' ranges considered for the parametric study. Table 1 shows Young's Modulus value ranges according to parametric points.

D. *Reduced Model*

The state-space full order model (FOM) has a total degree of freedom (DOF) of $N = 30{,}612$ as the system matrices size for the state-space model is $N \times N$. The reduced order model has a total DOF of $q = 8$ with reduced system matrices size $q \times q$. So, the simulation time required for the parametric reduced-order model is significantly less than FOM. The pMOR solution, including reduction processes, for seven parametric points only required $818s$, whereas the ANSYS solution would have required approximately $4305s$, performing simulations on the same computer. So, with the pMOR approach, an 81% reduction in computational time has been achieved.

A flow chart showing the organisational steps taken to carry out the pMOR study is shown in Fig. 5. The PEM model has been built in ANSYS for FEM discretisation. System matrices and load vectors have been extracted, from the ANSYS, for three parametric points ($\boldsymbol{p}_0$, $\boldsymbol{p}_3$ and $\boldsymbol{p}_6$) after the discretisation. These system matrices have been exported as sparse matrices for portability. The matrices and vectors have

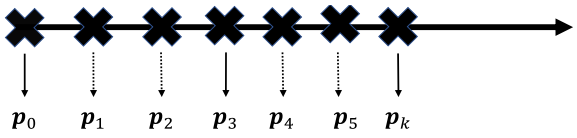

Figure 3: Uniform parametric points.

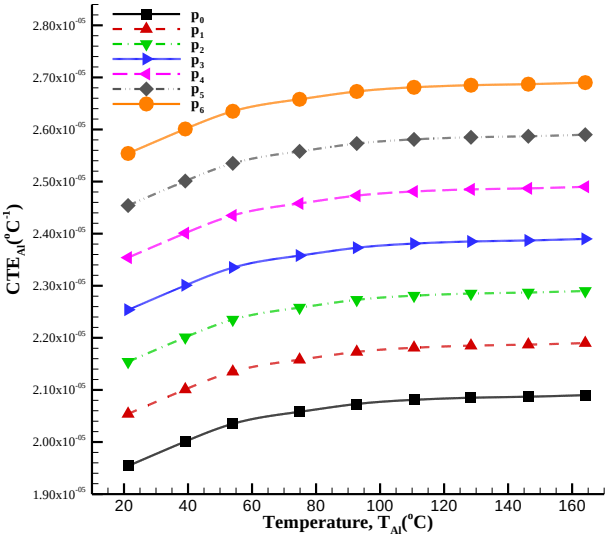

Figure 4: Parametric points for the temperature dependent coefficient of thermal expansion of Al (alloy), CTE_{Al}.

TABLE 1: PARAMETRIC POINTS FOR THE YOUNG'S MODULUS OF Al (ALLOY), E_{Al}.

Parametric Points	**Young's Modulus (E_{Al}) in GPa**
$\boldsymbol{p}_0$	71.06 GPa
$\boldsymbol{p}_1$	71.05 GPa
$\boldsymbol{p}_2$	71.04 GPa
$\boldsymbol{p}_3$	71.03 GPa
$\boldsymbol{p}_4$	71.02 GPa
$\boldsymbol{p}_5$	71.01 GPa
$\boldsymbol{p}_6$	71.00 GPa

been imported into MATLAB for the next step. With these matrices and vectors, a parametric reduced-order model has been built using the pMOR approach.

E. *Resutls and Discussions*

For carrying out the pMOR study with the current FEM discretised model, it is required that pMOR results agree well with the ANSYS full order model (FOM) solution. The degrees of freedom (DOFs) in the current model are

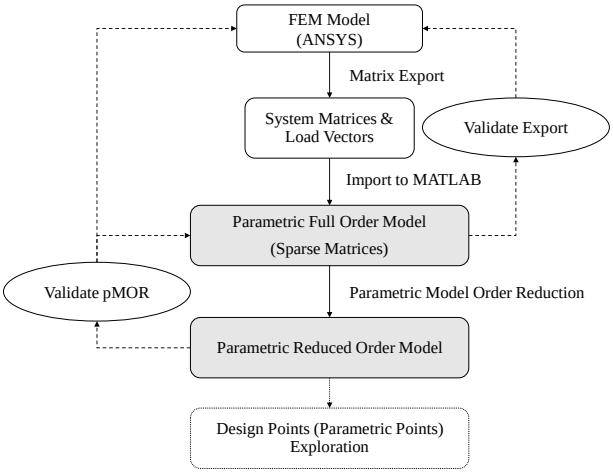

Figure 5: The organisational process for pMOR.

temperature and directional deformations, i.e., deformation in the x-axis and deformation in the y-axis. In Fig. 6s, the contours of temperature and total deformation distributions are shown considering the left part of the PEM structure. This figure compares results obtained from ANSYS solution against parametric reduced order model solution. Interpolated parametric point solution from the reduced order model has been compared here to validate the matrix interpolation method additionally. The chosen parametric point for the result shown in Fig. 6 is $\boldsymbol{p}_5$. The reduced order model solution agrees very well with the ANSYS solution.

Fig. 6(a) and 6(b) show that the temperature load in the wire bond area is one of the highest temperature regions of the model. The temperature in the wire bond area reaches the level of the temperature of the heat-generating body (*SiC*-based semiconductor). The peak values of the temperature distribution in the PEM structure have about a 0.04% difference between ANSYS and reduced order model solutions. This wire bond area is the area of interest for analyses in this work.

In Fig. 6(c) and 6(d), it is seen that the wire structure encounters the highest level of deformation in the module. The wire bond area of the PEM structure also sees a comparatively very high level of deformation. The difference in the peak value of the total deformation results between ANSYS and the reduced model's solution is approximately 1.4%. The highest deformation area in the PEM structure was anticipated to be in the wire structure for the considered model.

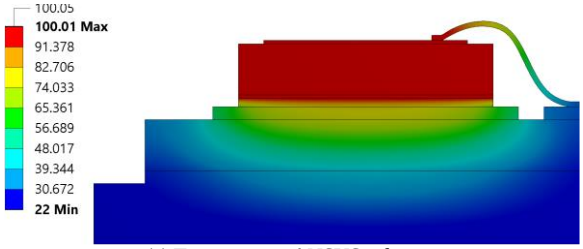

(a) Temperature, ANSYS solution.

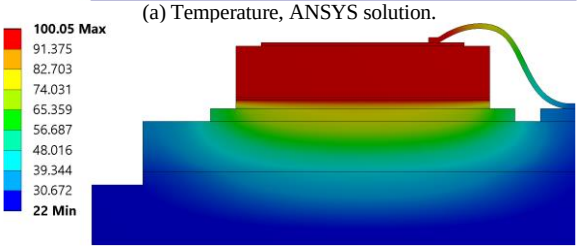

(b) Temperature, pMOR solution (interpolated).

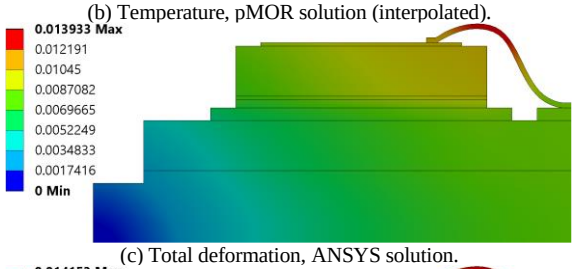

(c) Total deformation, ANSYS solution.

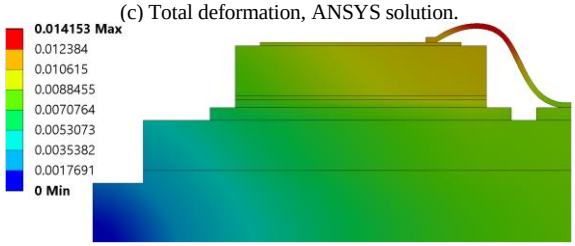

(d) Total deformation, pMOR solution (interpolated).

Figure 6: Temperature and Total Deformation distribution from ANSYS and pMOR solutions in the left part of the PEM structure for the parametric point $\boldsymbol{p}_5$.

Fig. 7 shows the equivalent (von-Mises) stress results in the wire bond region. Results for this figure are across a probing point, a line/path, as seen in Fig. 7(a). The probing point is in the wire structure's edge and in the wire structure, which is in direct contact with *Al* (alloy) layer adjacent to the

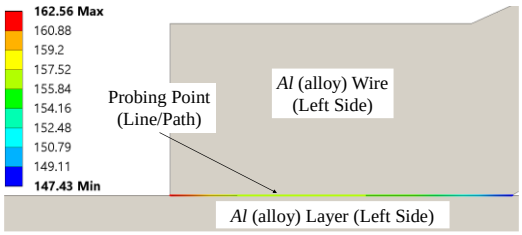

(a) Equivalent (von-Mises) stress, obtained by the pMOR solution, along the probing point (line/path) in PEM (Fig. 1) for parametric point $\boldsymbol{p}_5$.

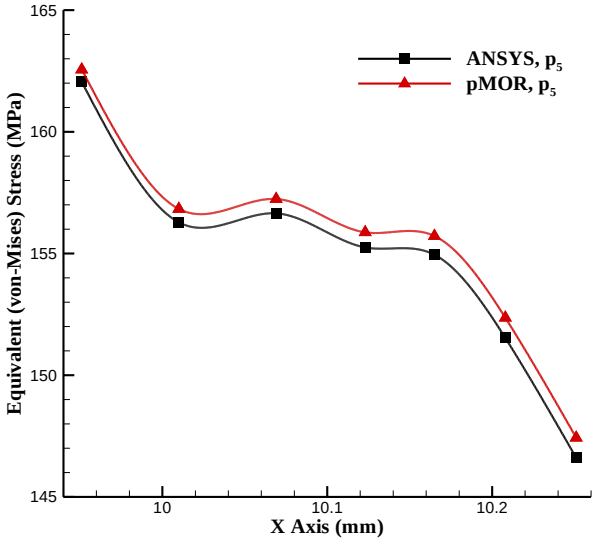

(b) Equivalent (von-Mises) stress, ANSYS vs pMOR solution, for the parametric point $\boldsymbol{p}_5$.

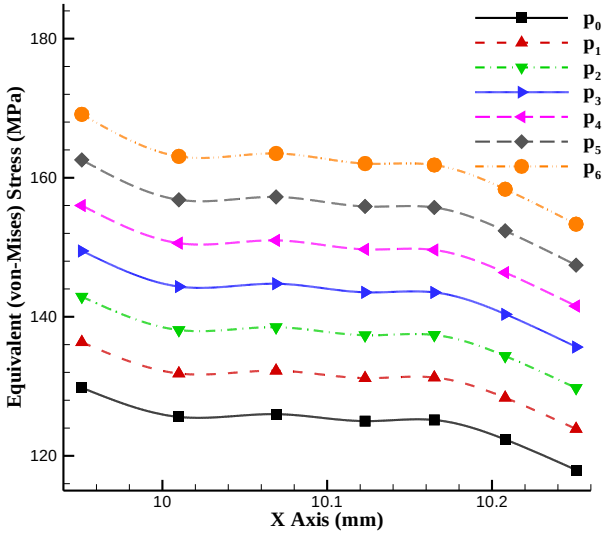

(c) Equivalent (von-Mises) stress, obtained by the pMOR solution, for all the considered parametric points.

Figure 7: Equivalent (von-Mises) stress along a probing point (line/path) in wire bond region of PEM structure shown in Fig. 1.

heat generating source, *SiC*-based semiconductor, to its opposite side. So, the results show the predicted stresses in the wire body for the considered probing point (line/path), considering the importance of this area [37, 38]. Fig. 7(b) compares stress results obtained from ANSYS and reduced order model solutions for the parametric point p_5, an interpolated parametric point for pMOR with matrix interpolation. The equivalent (von-Mises) stress result agrees very well with the ANSYS result. The stress results, shown in Fig. 7(b), have an average difference of only 0.43% between ANSYS and reduced-order model solutions. So, the reduced order modelling approach, pMOR, provides an excellent approximate model and is suitable for reliability analysis. In Fig. 7(c), equivalent stress results obtained by the reduced order model along the probing point are shown for all the parametric points. It is seen from the figure that equivalent (von-Mises) stresses along the probing point range approximately from $120MPa$ to $170MPa$ for considered parametric points. In the current model, the wire material, *Al* (alloy), has a yield strength of $280MPa$. So, the equivalent (von-Mises) stresses in the wire bond area do not exceed the yield strength of the material for analysed parametric points.

F. Error Analysis

The local reduced order model in (3) or the parametric reduced order model in (8) cannot be solved errors free. The model order reduction errors can be computed using the transfer functions of the full-order and reduced-order models. The error calculation method can be stated as the following [9, 19]:

$$\boldsymbol{\epsilon}(\boldsymbol{p}_i, s) = \frac{||\boldsymbol{Y}(\boldsymbol{p}_i, s) - \boldsymbol{Y}_r(\boldsymbol{p}_i, s)||}{||\boldsymbol{Y}(\boldsymbol{p}_i, s)||} \tag{14}$$

Table 2 shows the model order reduction error for the parametric point $\boldsymbol{p}_3$. Two different orders of the reduced model have been explored before further analysis. It is seen in Table 2 that order 8 and 9 show similar model order reduction error. Since the model order reduction error doesn't change much for the reduced order 9, the pMOR study has been carried out with reduced order 8.

IV. Conclusion

A parametric study has been carried out for a direct-coupled thermal-mechanical analysis of a power electronics module. The parametric study has been conducted using the parametric model order reduction method. The temperature-dependent values of the coefficient of thermal expansion and constant values of Young's modulus of the wire structure have been parametrised for parametric/design point exploration. The Krylov subspace-based approach PRIMA has been used for model order reduction, and the bi-linear technique of matrix interpolation has been used to build a parametric reduced-order model. The reduced order model has very low dimensionality and saves a significant amount of computational time, about 81%. The reduced order model retains a very high level of accuracy, showing only a 0.43% difference in the stress result. Overall, the pMOR method offered in this work can overcome any challenges related to simulation time that may arise during reliability analysis-based design explorations while considering a large-scale model. Further studies will be focused on implementing pMOR approaches considering models with nonlinear plasticity behaviours in the wire material.

TABLE 2: Model Order Reduction Error for the Parametric Point $\boldsymbol{p}_3$.

Order of the Reduced Model	Error, $\boldsymbol{\epsilon}(\boldsymbol{p}_3, \boldsymbol{t})$
8	2.8446×10^{-4}
9	2.8083×10^{-4}

References

[1] G. Dhatt, E. Lefrançois and G. Touzot, Finite element method, John Wiley & Sons, 2012.

[2] P. Rajaguru, H. Lu and C. Bailey, "Sintered silver finite element modelling and reliability based design optimisation in power electronic module," *Microelectronics Reliability*, vol. 55, no. 6, pp. 919-930, 2015.

[3] T. Himika, S. Hassan, M. Hasan and M. Molla, "Lattice Boltzmann Simulation of MHD Rayleigh–Bénard Convection in Porous Media," *Arabian Journal for Science and Engineering*, vol. 45, no. 11, pp. pp.9527-9547, 2020.

[4] S. Hassan, D. Redwan, M. Molla, S. Thohura, M. Taher and S. Siddiqa, "A Study on Heat Transfer Enhancement through Various Nanofluids in a Square Cavity with Localized Heating," *Energy Engineering*, vol. 118, no. 6, pp. 1659-1679, 2021.

[5] A. Rahman, P. Nag, M. Molla and S. Hassan, "Magnetic field effects on natural convection and entropy generation of non-Newtonian fluids using multiple-relaxation-time lattice Boltzmann method," *International Journal of Modern Physics C*, vol. 32, no. 01, p. p.2150015, 2021.

[6] T. Himika, S. Hassan, M. Hasan, M. Molla, M. Taher and S. Saha, "Lattice boltzmann simulation of magnetic field effect on electrically conducting fluid at inclined angles in rayleigh-bénard convection," *Energy Engineering*, vol. 118, no. 1, p. 15–36, 2021.

[7] E. Davison, "A method for simplifying linear dynamic systems," *IEEE Transactions on automatic control*, vol. 11, no. 1, pp. 93-101, 1966.

[8] R. W. Freund, "Model reduction methods based on Krylov subspaces," *Acta Numerica*, vol. 12, pp. 267-319, 2003.

[9] P. Rajaguru, M. Bella and C. Bailey, "Applying Model Order Reduction to the Reliability Prediction of Power Electronic Module Wirebond Structure," in *2021 27th International Workshop on Thermal Investigations of ICs and Systems (THERMINIC)*, 2021.

[10] M. Eblen, "Applied FEM techniques in ceramic feedthru package design," in *2004 Proceedings. 54th Electronic Components and Technology Conference (IEEE Cat. No. 04CH37546)*, 2004.

[11] L. Codecasa, A. Di Costanzo, V. d'Alessandro, R. Duca, D. Gualandris, A. Morelli, F. De Viti and C. Villa, "Towards the Extension of TRIC for Thermo-Mechanical Analysis," in *2021 27th International Workshop on Thermal Investigations of ICs and Systems (THERMINIC)*, 2021.

[12] F. Shen and L. Ke, "Numerical study of coupled electrical-thermal-mechanical-wear behavior in electrical contacts.," *Metals*, vol. 11, no. 6, p. 955, 2021.

[13] Z. Bai and Y. Su, "Dimension reduction of large-scale second-order dynamical systems via a second-order Arnoldi method.," *SIAM Journal on Scientific Computing*, vol. 26, no. 5, pp. 1692-1709, 2005.

[14] W. Liu, H. Torsten and J. Drobnik, "Effective Thermal Simulation of Power Electronics in Hybrid and Electric Vehicles," *World Electric Vehicle Journal*, vol. 5, no. 2, pp. 574-580, 2012.

[15] L. Codecasa, R. Bornoff, J. Dyson, V. d'Alessandro, A. Magnani and N. Rinaldi, "Versatile MOR-based boundary condition independent compact thermal models with multiple heat sources," *Microelectronics Reliability*, vol. 87, pp. 194-205, 2018.

[16] B. Rogié, L. Codecasa, E. Monier-Vinard, V. Bissuel, N. Laraqi, O. Daniel, D. D'Amore, A. Magnani, V. d'Alessandro and N. Rinaldi, "Multi-port dynamic compact thermal models of dual-chip package using model order reduction and metaheuristic optimization," *Microelectronics Reliability*, vol. 87, pp. 222-231, 2018.

[17] L. Codecasa, V. d'Alessandro and D. D'Amore, "Altering MOR-based BCI CTMs into Delphi-like BCI CTMs," 2020.

[18] J. Choi, M. Cho and J. Rhim, "Efficient prediction of the quality factors of micromechanical resonators," *Journal of Sound and Vibration*, vol. 329, no. 1, pp. 84-95, 2010.

[19] P. Rajaguru, H. Lu, C. Bailey and M. Bella, "Modelling and analysis of vibration on power electronic module structure and application of model order reduction," *Microelectronics*, vol. 110, p. 113697, 2020.

[20] V. Bissuel, V. Fox, E. Monier-Vinard, A. Neveu, F. Joly and O. Daniel, "Multi-port Dynamic Compact Thermal Models of BGA package using Model Order Reduction and Metaheuristic Optimization.," in *2019 18th IEEE Intersociety Conference on Thermal and Thermomechanical Phenomena in Electronic Systems (ITherm)*, 2019.

[21] U. Baur, P. Benner, B. Haasdonk, C. Himpe, I. Maier and M. Ohlberger, "Comparison of methods for parametric model order reduction of instationary problems," *Max Planck Institute for Dynamics of Complex Technical Systems*, 2015.

[22] L. Feng, Y. Yue, N. Banagaaya, P. Meuris, W. Schoenmaker and P. Benner, "Parametric modeling and model order reduction for (electro-) thermal analysis of nanoelectronic structures," *Journal of Mathematics in Industry*, vol. 6, no. 1, pp. 1-16, 2016.

[23] E. ter Maten, P. Putek, M. Günther, R. Pulch, C. Tischendorf, C. Strohm, W. Schoenmaker, P. Meuris, B. De Smedt, P. Benner and L. Feng, "Nanoelectronic COupled problems solutions-nanoCOPS: modelling, multirate, model order reduction, uncertainty quantification, fast fault simulation.," *Journal of Mathematics in Industry*, vol. 7, no. 1, pp. 1-19, 2016.

[24] S. Bouhedma, Y. Rao, A. Schütz, C. Yuan, S. Hu, F. Lange, T. Bechtold and D. Hohlfeld, "System-level model and simulation of a frequency-tunable vibration energy harvester," *Micromachines*, vol. 11, no. 1, p. 91, 2020.

[25] A. Schütz, M. Olbrich, S. Hu, C. Ament and T. Bechtold, "Parametric system-level models for position-control of novel electromagnetic free flight microactuator," *Microelectronics Reliability*, p. 114062, 2021.

[26] C. Yuan, D. Hohlfeld and T. Bechtold, "Design optimization of a miniaturized thermoelectric generator via parametric model order reduction.," *Microelectronics Reliability*, vol. 119, p. 114075, 2021.

[27] C. Scognamillo, A. Catalano, M. Riccio, V. d'Alessandro, L. Codecasa, A. Borghese, R. Tripathi, A. Castellazzi, G. Breglio and A. Irace, "Compact Modeling of a 3.3 kV SiC MOSFET Power Module for Detailed Circuit-Level Electrothermal Simulations Including Parasitics," *Energies*, vol. 14, no. 15, p. 4683, 2021.

[28] A. Schütz, S. Maeter and T. Bechtold, "System-Level Modelling and Simulation of a Multiphysical Kick and Catch Actuator System," *Actuators*, vol. 10, no. 11, p. 279, 2021.

[29] H. Panzer, J. Mohring, R. Eid and B. Lohmann, "Parametric model order reduction by matrix interpolation," *Automatisierungstechnik*, vol. 58, no. 8, pp. 475-484, 2010.

[30] A. Odabasioglu, M. Celik and L. Pileggi, "PRIMA: Passive reduced-order interconnect macromodeling algorithm.," *IEEE Transactions on computer-aided design of integrated circuits and systems*, vol. 17, no. 8, pp. 645-654, 1998.

[31] S. Race, A. Philipp, M. Nagel, T. Ziemann, I. Kovacevic-Badstuebner and U. Grossner, "Circuit-based electrothermal modeling of SiC power modules with nonlinear thermal models," *IEEE Transactions on Power Electronics*, vol. 37, no. 7, pp. 7965-7976, 2022.

[32] M. Geuss, H. Panzer and B. Lohmann, "On parametric model order reduction by matrix interpolation," in *2013 European Control Conference (ECC)*, 2013.

[33] M. Geuss, D. Butnaru, B. Peherstorfer, H. Bungartz and B. Lohmann, "Parametric model order reduction by sparse-grid-based interpolation on matrix manifolds for multidimensional parameter spaces," in *2014 European Control Conference (ECC)*, 2014.

[34] B. Lohmann and B. Salimbahrami, "Reduction of second order systems using second order Krylov subspaces," in *IFAC Proceedings Volumes*, 2005.

[35] ANSYS, *Mechanical APDL 2023 R1 - Theory Reference*, ANSYS, 2023.

[36] S. Lachance-Barrett and K. Alexander, *Wind Turbine Blade FSI (Part 2)—Mesh*, Ithaca, NY, USA: Cornell University, 2018.

[37] C. Bailey, T. Tilford and H. Lu, "Reliability analysis for power electronics modules," in *2007 30th International Spring Seminar on Electronics Technology (ISSE)*, 2007.

[38] K. Nwanoro, H. Lu, C. Yin and C. Bailey, "Advantages of the extended finite element method for the analysis of crack propagation in power modules," *Power Electronic Devices and Components*, vol. 4, p. 100027, 2023.